



HAL
open science

A New Theoretical Framework for Characterizing the Transport of Liquid in Turbulent Two-Phase Flows

Fabien Thiesset, Thibaut Ménard, Christophe Dumouchel

► **To cite this version:**

Fabien Thiesset, Thibaut Ménard, Christophe Dumouchel. A New Theoretical Framework for Characterizing the Transport of Liquid in Turbulent Two-Phase Flows. ILASS-Europe, Sep 2019, Paris, France. hal-02271685

HAL Id: hal-02271685

<https://normandie-univ.hal.science/hal-02271685>

Submitted on 13 Sep 2019

HAL is a multi-disciplinary open access archive for the deposit and dissemination of scientific research documents, whether they are published or not. The documents may come from teaching and research institutions in France or abroad, or from public or private research centers.

L'archive ouverte pluridisciplinaire **HAL**, est destinée au dépôt et à la diffusion de documents scientifiques de niveau recherche, publiés ou non, émanant des établissements d'enseignement et de recherche français ou étrangers, des laboratoires publics ou privés.

A new theoretical framework for characterizing the transport of liquid in turbulent two-phase flows

F. Thiesset^{1*}, T Ménard², C. Dumouchel¹

¹ CNRS, CORIA UMR 6614, Rouen Normandy University, INSA Rouen, Avenue de l'université, 76801 Saint Etienne du Rouvray, FRANCE

² Rouen Normandy University, CORIA UMR 6614, CNRS, INSA Rouen, Avenue de l'université, 76801 Saint Etienne du Rouvray, FRANCE

*Corresponding author: fabien.thiesset@coria.fr

Abstract

When a liquid stream is injected into a gaseous atmosphere, it destabilizes and continuously passes through different states characterized by different morphologies. Throughout this process, the flow dynamics may be different depending on the region of the flow and the scales of the involved liquid structures. Exploring this multi-scale, multi-dimensional phenomenon requires some new theoretical tools, some of which need yet to be elaborated. In the present study, an innovative general framework is established by transposing the machinery of two-point statistical analysis to a relevant metric of liquid-gas flows (the liquid volume fraction). This allows distinguishing the transport of liquid which occurs in geometrical space (i.e. from one position in the flow to the other) and the one occurring in scale space (e.g. from large to small scales). These equations are exact and do not rely on any particular assumptions. The notion of scale is explicit and unambiguously defined. They further apply to the entire flow field, from the injection to the spray dispersion zone and irrespectively of the flow configuration or regime. This new set of equations is here invoked to characterize the air-assisted atomization of a planar liquid layer simulated by means of Direct Numerical Simulation using the ARCHER code.

Keywords

Atomization, Volume-of-Fluid, Two-point equations

Introduction

According to Villermaux [22], there exist three classes of theoretical elaborations for describing the atomization of liquid streams: the sequential cascade models, the aggregation models, and the maximum entropy formalism. The first class of elaborations dates back to Kolmogorov [11] and considers the atomization process as a successive reduction of 'mother drops' into a hierarchy of smaller 'daughter drops'. This approach in its original and modern versions [4] thus conceptualizes the atomization process as a cascade mechanism, analogous to single fluid turbulence [9], where the sense of evolution is directed towards small scales. The second class of models is due mainly to the work by Villermaux and co-workers [23, 12]. They postulated that droplets emanate from the rupture of detached ligaments which are formed during the primary atomization process. These ligaments are assumed to be virtually constituted of spherical blobs, which successively aggregate yielding a given droplet size distribution in the spray. Hence, opposite to the cascade models, the aggregation scenario indicates that the transfer among the different scales is directed towards the large scales. Finally, the last class of theory relies on the Maximum Entropy Formalism [18, 3]. The idea is to consider, again, the liquid as being constituted as a set of elementary bricks and to compute the most probable distribution of disjoint clusters given some constraints that are imposed on the system. In the Maximum Entropy Formalism, the process of cluster formation is done in one step and there is no explicit description of the underlying dynamics or kinematics.

All aforementioned models emphasize the cornerstone notion of constitutive scale (mother and daughter drops, blobs). However, in both vision, this notion is invoked ex nihilo and lacks of robust mathematical foundation. If a typical scale were to be unambiguously defined, it could only correspond to the diameter of a sphere (ligament) even though the liquid structures are generally far from being spherical (cylindrical) in the secondary atomization zone. Consequently, the ambiguity in the definitions for the constitutive scales implies notably different postulates for the direction of transfer in scale-space, although it remains very unclear in which particular direction, if one were to exist, the evolution preferentially occurs [5]. Another direct consequence is that predictions of such theories can be tested mostly in the very far field of the spray, where droplets are spherical for the 'drop-size' to be defined and measured. Therefore, they cannot be validated in the region of the flow where the processes they are describing are acting. Last but not least, these theories cannot conclude about the existence of a scale, as numerically evidenced in [13], below which the atomization process may stop. For example, the cascade model implicitly considers atomization at large Weber numbers (the surface tension force tends to zero) in which case the atomization process a priori never ceases and droplets of infinitely small size can possibly be created [4]. To circumvent this limitation in the model, the atomization process is artificially interrupted when drops become smaller than a critical value based on dimensional arguments.

Besides two-phase flows, the concept of hierarchized scales among which energy is transferred has been extensively explored in the context of single phase turbulent flows. This idea dates back to Richardson [16] and has deeply inspired von Kármán & Howarth [8] and Kolmogorov [10] who were first to derive the transport equations for

the two-point statistics, i.e. correlation or structure functions of observables such as the velocity field. Yaglom [24] derived similar equations for a passive scalar such as temperature. Considering an analysis of the relevant metrics (e.g. velocity, temperature, concentration) not only at one point but at two points in space allows to mathematically define the notion of scale as the straight distance between the two points considered. In the last two decades, generalizations of the Kármán-Howarth-Kolmogorov or Yaglom equations, have emerged where the assumption of statistical homogeneity and isotropy are relaxed [2, 6, 19]. In addition to unambiguously define the notion of scale, the main benefit of such two-point equations is that they allow to evaluate and distinguish the processes (production / diffusion / transfer) occurring in the geometrical space (i.e. from one position in the flow to the other) from that taking place in scale space (from e.g. large to small scales).

In the present study, the machinery of two-point statistical analysis is adapted to a relevant metric of two-phase flows with the goal of exploring the transport of liquid in both scale and geometrical space. The scalar of interest is here the liquid volume fraction. It is linked to the the volume-of-fluid which is widely used in numerical simulations to characterize the evolution of the liquid-gas interface [7, 17]. Our objectives in deriving such a new framework is to provide insights into (i) the direction and amplitude of the transfer among the different scales during liquid-atomization, (ii) the existence of a cut-off scale below which atomization ceases and (iii) the effect of different physical parameters (surface tension, viscosity and density, inflow velocity conditions), and the range of scales over which these parameters have an influence. Only point (i) is addressed here. Although this framework applies irrespectively of the investigated zone within the flow and independently of the injection regime, focus is shed here on the air-assisted atomization of a planar liquid layer.

This paper is organized as follows. First, the derivation of the two-point statistical equations for the liquid fraction field are presented. Second, the numerical simulations used throughout this study are presented. Finally, results of the application of the new theoretical framework to air-assisted atomization are discussed. Conclusions are drawn in a last section.

Analytical considerations

The liquid volume fraction ϕ designates the portion of liquid contained within a given volume (generally the mesh cell). $\phi = 1$ if cells contain only liquid, $\phi = 0$ if they contain only gas and $0 < \phi < 1$ if a liquid-gas interface crosses the volume under consideration. An example of such a field function is portrayed in Fig. 1(a). For non evaporating liquids in incompressible flows, its transport equation reads

$$\partial_t \phi + \mathbf{u} \cdot \nabla_{\mathbf{x}} \phi = 0 \quad (1)$$

where $\partial_t \equiv \partial/\partial t$ and $\nabla_{\mathbf{x}}$ is the gradient operator with respect to the coordinate \mathbf{x} . The equation for ϕ is therefore that of a non-diffusive passive scalar. The effect of viscosity and density jumps together with surface tension of the liquid-gas interface is implicit through the appearance of the velocity field $\mathbf{u}(\mathbf{x}, t)$.

The algebra for deriving the two-point equations of ϕ is similar to what was presented in e.g. [6, 2] for the velocity field and is reproduced here. Eq. (1) is first written at a point \mathbf{x}^+ and a point \mathbf{x}^- arbitrarily separated by a distance r (see Fig. 1(a))

$$\partial_t \phi^\pm + \mathbf{u}^\pm \cdot \nabla_{\mathbf{x}^\pm} \phi^\pm = 0 \quad (2)$$

where superscript plus (minus) denote the quantity at point \mathbf{x}^+ (\mathbf{x}^-). Taking the difference of Eq. (2) between the two points considered yields

$$\partial_t (\phi^+ - \phi^-) + \mathbf{u}^+ \cdot \nabla_{\mathbf{x}^+} \phi^+ - \mathbf{u}^- \cdot \nabla_{\mathbf{x}^-} \phi^- = 0 \quad (3)$$

For any quantity β , we have $\nabla_{\mathbf{x}^-} \beta^+ \equiv \nabla_{\mathbf{x}^+} \beta^- \equiv 0$. Using the continuity equation $\nabla_{\mathbf{x}^+} \cdot \mathbf{u}^+ = \nabla_{\mathbf{x}^-} \cdot \mathbf{u}^- = 0$, Eq. (3) can then be rewritten as

$$\partial_t \delta\phi + \nabla_{\mathbf{x}^+} \cdot \mathbf{u}^+ \delta\phi + \nabla_{\mathbf{x}^-} \cdot \mathbf{u}^- \delta\phi = 0 \quad (4)$$

where $\delta\beta = \beta^+ - \beta^- = \beta(\mathbf{x}^+, t) - \beta(\mathbf{x}^-, t)$ is the increment (the difference) of the quantity β between the two points \mathbf{x}^+ and \mathbf{x}^- . Let $\mathbf{X} = (\mathbf{x}^+ + \mathbf{x}^-)/2$ being the midpoint and $\mathbf{r} = (\mathbf{x}^+ - \mathbf{x}^-)$ the separation vector between \mathbf{x}^+ and \mathbf{x}^- (Fig. 1(a)). The gradient with respect to \mathbf{X} and \mathbf{r} are then related to $\nabla_{\mathbf{x}^-}$ and $\nabla_{\mathbf{x}^+}$ by

$$\nabla_{\mathbf{x}^\pm} = \pm \nabla_{\mathbf{r}} + \frac{1}{2} \nabla_{\mathbf{X}} \quad (5)$$

Explanations for choosing \mathbf{X} and \mathbf{r} instead of \mathbf{x}^+ and \mathbf{x}^- are given in [6]. Injecting Eqs. (5) into Eq. (4) leads to

$$\partial_t \delta\phi + \nabla_{\mathbf{r}} \cdot \delta\mathbf{u} \delta\phi + \nabla_{\mathbf{X}} \cdot \sigma\mathbf{u} \delta\phi = 0 \quad (6)$$

where $\sigma\beta = \frac{1}{2}(\beta^+ + \beta^-)$ is the average of the quantity β between the two points \mathbf{x}^+ and \mathbf{x}^- . Multiplying Eq. (6) by $\delta\phi$ yields

$$\partial_t (\delta\phi)^2 + \nabla_{\mathbf{r}} \cdot \delta\mathbf{u} (\delta\phi)^2 + \nabla_{\mathbf{X}} \cdot \sigma\mathbf{u} (\delta\phi)^2 = 0 \quad (7)$$

The quantity under consideration in Eq. (7) is $(\delta\phi)^2$, the squared difference of ϕ between two arbitrary points. $(\delta\phi)^2$ is non zero only if the liquid-gas interface is present between the two points considered. As a consequence, $(\delta\phi)^2(\mathbf{X}, \mathbf{r}, t)$ is somehow related to the probability of finding the liquid gas interface between two points separated by a distance r . At large separations, this probability is larger than for small separations, so that $(\delta\phi)^2$ is expected to be an increasing function of $|\mathbf{r}|$.

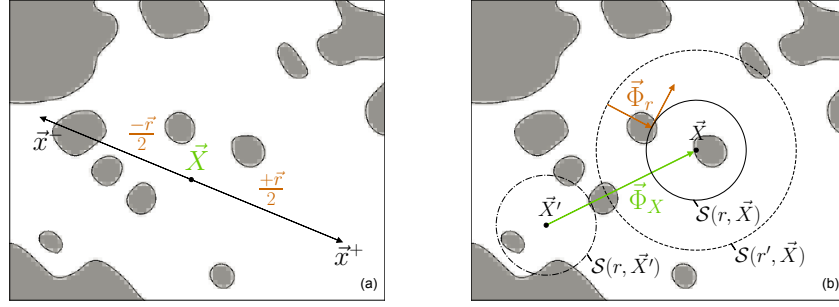


Figure 1. (a) Example of liquid volume fraction field. Dark regions correspond to the liquid-phase and white regions to the gas-phase. The interface is also displayed as black curves. The two-points x^+ and x^- used to calculate increments are portrayed together with the midpoint \mathbf{X} and the separation vector \mathbf{r} . (b) Schematic representation of the flux $\Phi_{\mathbf{r}}$ and $\Phi_{\mathbf{X}}$

Equation for the fluctuating component

Because the flows under consideration are generally turbulent, it is convenient to decompose ϕ and \mathbf{u} into a mean (Reynolds average) and a fluctuating component before proceeding to average. The type of averaging procedure depends on the flow configuration and will be detailed later. The mean and fluctuating part of the fields under consideration are given by

$$\phi = \bar{\phi} + \phi' \quad (8a)$$

$$\mathbf{u} = \bar{\mathbf{u}} + \mathbf{u}' \quad (8b)$$

By definition, the averaged fluctuations $\overline{\mathbf{u}'}, \overline{\phi'} \equiv 0$. The equations for $\overline{(\delta\phi)^2}$ and $\overline{(\delta\phi')^2}$ are obtained multiplying Eq. (6) by $\delta\bar{\phi}$ and $\delta\phi'$, respectively, and then proceed to average. For the fluctuating component, one obtains

$$\begin{aligned} \partial_t \overline{(\delta\phi')^2} + \nabla_{\mathbf{r}} \cdot \left(\delta\bar{\mathbf{u}} \overline{(\delta\phi')^2} + \delta\mathbf{u}' \overline{(\delta\phi')^2} \right) + 2\overline{\delta\phi' \delta\mathbf{u}'} \cdot \nabla_{\mathbf{r}} \delta\bar{\phi} \\ + \nabla_{\mathbf{X}} \cdot \left(\sigma\bar{\mathbf{u}} \overline{(\delta\phi')^2} + \sigma\mathbf{u}' \overline{(\delta\phi')^2} \right) + 2\overline{\delta\phi' \sigma\mathbf{u}'} \cdot \nabla_{\mathbf{X}} \delta\bar{\phi} = 0 \end{aligned} \quad (9)$$

Eq. (9) can be formally rewritten as

$$\partial_t \overline{(\delta\phi')^2} = \underbrace{-\nabla_{\mathbf{r}} \cdot \Phi_{\mathbf{r}}}_{\text{Transfer } \mathbf{r}} - \underbrace{\nabla_{\mathbf{X}} \cdot \Phi_{\mathbf{X}}}_{\text{Transfer } \mathbf{X}} - \underbrace{\Pi_{\mathbf{r}}}_{\text{Production } \mathbf{r}} - \underbrace{\Pi_{\mathbf{X}}}_{\text{Production } \mathbf{X}} \quad (10)$$

In addition to a non-stationary term, Eq. (10) reveals two flux terms, in the \mathbf{r} - and \mathbf{X} -space, respectively. These are expressed as follows

$$\Phi_{\mathbf{r}} = \delta\bar{\mathbf{u}} \overline{(\delta\phi')^2} + \delta\mathbf{u}' \overline{(\delta\phi')^2} = \delta\mathbf{u} \overline{(\delta\phi')^2} \quad (11a)$$

$$\Phi_{\mathbf{X}} = \sigma\bar{\mathbf{u}} \overline{(\delta\phi')^2} + \sigma\mathbf{u}' \overline{(\delta\phi')^2} = \sigma\mathbf{u} \overline{(\delta\phi')^2} \quad (11b)$$

$\nabla_{\mathbf{r}}$ and $\nabla_{\mathbf{X}}$ are the gradient operator in \mathbf{r} - and \mathbf{X} -space, respectively. Therefore, $\nabla_{\mathbf{r}} \cdot \Phi_{\mathbf{r}}$ and $\nabla_{\mathbf{X}} \cdot \Phi_{\mathbf{X}}$ are characteristic of a transfer process occurring in the \mathbf{r} - and \mathbf{X} -space, respectively. More precisely, the term $\Phi_{\mathbf{r}}$ represents the flux of the fluctuating quantity $(\delta\phi')^2$ from spherical shells $\mathcal{S}(r, \mathbf{X})$ (see Fig. 1 (b)) centred at \mathbf{X} with radius $r = |\mathbf{r}|$ either to spherical shells centred at the same \mathbf{X} but with different radius r' or within the same spherical shell but to a different orientation \mathbf{r}/r . This flux operates with a characteristic velocity $\delta\mathbf{u} = \delta\bar{\mathbf{u}} + \delta\mathbf{u}'$, i.e. the sum of mean and fluctuating velocity increments. On the other hand, the term $\Phi_{\mathbf{X}}$ represents the flux of the fluctuating quantity $(\delta\phi')^2$ from spherical shells $\mathcal{S}(r, \mathbf{X})$ (see Fig. 1 (b)) centred at \mathbf{X} with radius $r = |\mathbf{r}|$ to a spherical shell of same size centered at another point in flow-position space \mathbf{X}' . The latter is driven by a characteristic velocity $\sigma\mathbf{u} = \sigma\bar{\mathbf{u}} + \sigma\mathbf{u}'$, i.e. the sum of mean and fluctuating velocity half sum.

Eq. (10) also contains two terms which are usually interpreted as some production terms due to gradient of mean quantities in the \mathbf{r} - and \mathbf{X} -space, respectively

$$\Pi_{\mathbf{r}} = 2\overline{\delta\mathbf{u}' \delta\phi'} \cdot \nabla_{\mathbf{r}} \delta\bar{\phi} \quad (12a)$$

$$\Pi_{\mathbf{X}} = 2\overline{\sigma\mathbf{u}' \delta\phi'} \cdot \nabla_{\mathbf{X}} \delta\bar{\phi} \quad (12b)$$

$\Pi_{\mathbf{r}}$ and $\Pi_{\mathbf{X}}$ characterize the exchanges of energy from the mean field to the fluctuating component. In summary, Eq. (10) reveals that $\overline{(\delta\phi')^2}$ changes in time due to (i) a production mechanism associated with statistical inhomogeneity of mean quantities, and (ii) redistribution through fluxes in both scale-space \mathbf{r} and position space \mathbf{X} . Contrary to the well known equation for the scalar field such as temperature or pollutant concentration (i.e. the generalised Yaglom equation, see e.g. [1, 19]), ϕ is a non diffusive scalar. Therefore, the diffusion term and the scalar dissipation rate do not appear in Eq. (10). This is a very noticeable peculiarity of the liquid volume fraction.

As per [15], it is also convenient to define the convection velocities $\mathbf{w}_{\mathbf{r}, \mathbf{X}}$ in either the \mathbf{r} - or \mathbf{X} -space, i.e. $\overline{\delta\mathbf{u}} \overline{(\delta\phi')^2} = \mathbf{w}_{\mathbf{r}} \overline{(\delta\phi')^2}$ and $\overline{\sigma\mathbf{u}} \overline{(\delta\phi')^2} = \mathbf{w}_{\mathbf{X}} \overline{(\delta\phi')^2}$ which allows decomposing the transfer terms as

$$\nabla_{\mathbf{r}} \cdot \overline{\delta\mathbf{u}} \overline{(\delta\phi')^2} = \mathbf{w}_{\mathbf{r}} \cdot \nabla_{\mathbf{r}} \overline{(\delta\phi')^2} + \overline{(\delta\phi')^2} \nabla_{\mathbf{r}} \cdot \mathbf{w}_{\mathbf{r}} \quad (13a)$$

$$\nabla_{\mathbf{X}} \cdot \overline{\sigma\mathbf{u}} \overline{(\delta\phi')^2} = \mathbf{w}_{\mathbf{X}} \cdot \nabla_{\mathbf{X}} \overline{(\delta\phi')^2} + \overline{(\delta\phi')^2} \nabla_{\mathbf{X}} \cdot \mathbf{w}_{\mathbf{X}} \quad (13b)$$

Writing the transfer term in the form provided by Eqs. (13) allows highlighting an advection term with convection velocity $w_{r,\mathbf{X}}$ whose sign indicates the direction of the flux (negative/positive when directed towards smaller/larger scales), and a sink/source term accounting for the non solenoidal character of $w_{r,\mathbf{X}}$. From Eq. (13) it is then possible writing Eq. (10) in Lagrangian form revealing that variations of $(\delta\phi')^2$ along the trajectories of the field $w_{r,\mathbf{X}}$ are due to the combined effect of production $\Pi_{r,\mathbf{X}}$ and a sink/source term associated with $\nabla_{r,\mathbf{X}} \cdot w_{r,\mathbf{X}}$ being non zero.

To further elaborate on the origin of the source term $(\delta\phi')^2 \nabla_{r,\mathbf{X}} \cdot w_{r,\mathbf{X}}$, it is worth applying an Hodge-Helmholtz decomposition to $w_{r,\mathbf{X}}$. The velocity $w_{r,\mathbf{X}}$ can then be decomposed as the sum of a divergence-free (solenoidal) and a curl-free (irrotational) component. For w_r this writes as

$$w_r = -\nabla_r P_r + \nabla_r \wedge A_r \quad (14)$$

where P_r and A_r are the scalar and vector potential, respectively. The source term $f_r = \nabla_r \cdot w_r$ can thus be expressed in the form of a Poisson equation, viz. $f_r = -\nabla_r^2 P_r$. Using Green's function for Poisson's equation on an unbounded space and assuming that f_r decays faster than $|\mathbf{r}|^{-1}$ at large r , the solution for the scalar potential is given by

$$P_r = \iiint_{r'} G_r(\mathbf{r}' - \mathbf{r}) f_r(\mathbf{r}') d\mathbf{r}' \quad (15)$$

$G_r(\mathbf{r}' - \mathbf{r}) = \{4\pi|\mathbf{r}' - \mathbf{r}|\}^{-1}$, the Newtonian potential, describes the response of the system at scale r to a point source located at a larger scale r' . A similar interpretation applies to $w_{\mathbf{X}}$ in geometrical space. Writing the sink/source term in the form of a Poisson's equation therefore suggests that a given scale (or position) interact with all others scales (positions) through a scalar potential field. The sink/source term in Eq. (13) therefore contains information about the non-local character of the interactions between different scales or positions (a similar reasoning was elaborated as regards to the non-local effect of pressure in incompressible turbulence, see [20] p. 28). In other words, Eq. (13) can be seen as a way of decomposing the transfer terms into local and non-local processes. The left-most term on RHS of Eq. (13) characterizes local interactions between two neighbouring scales r or positions \mathbf{X} . Such interactions are made through a local transport process. On the other hand, the rightmost term on RHS of Eq. (13) emphasizes that there exists a potential field $P_{r,\mathbf{X}}$ which allow separated scales (or positions) to interact.

Details of the numerical simulations

The different terms of Eq. (10) are quantified from Direct Numerical Simulations (DNS) data using the ARCHER code [14]. This study has benefited from the latest developments of the code, notably the Rudman type solver allowing for a consistent transport of mass and momentum. The reader is referred to [21] for more details. The flow configuration is that of a planar liquid layer being sheared by a gas stream. The liquid and gas properties correspond to that of water and air at ambient pressure. The liquid was set to be at rest while the gas velocity is $u_g = 7.5 \text{ m.s}^{-1}$ flowing the x direction. The calculation domain is $L_x \times L_y \times L_z = 8 \times 4 \times 4 \text{ cm}^3$ in the streamwise, vertical and spanwise direction respectively, and the mesh size consisted of $N_x \times N_y \times N_z = 512 \times 256 \times 256$ cells. The liquid layer is $L_y/2$ thick. Close to the liquid-gas interface, an error function profile for the streamwise velocity is prescribed with a vorticity thickness of 1.15 mm. This was set so that the most unstable wavelength of the Kelvin-Helmholtz instability is expected to be half of L_x and the spanwise instability has a wavelength of about $L_z/6$. To facilitate the destabilization of the liquid layer and consequently reduce the overall computational time, we superimposed to the liquid-gas interface a small sinusoidal perturbation with period $L_x/2$ and $L_z/6$ in the streamwise and spanwise directions, respectively. Periodic boundary conditions are used in the streamwise and spanwise direction. A no-slip boundary condition is applied to the bottom frontier while an outflow condition is used at the uppermost boundary of the calculation domain.

The flow is statistically homogeneous along the x and z directions. One-point and two-point statistics are thus averaged along these directions, i.e. the appropriate average operation here writes

$$\bar{\beta} = \frac{1}{L_x L_z} \iint \beta dx dz \quad (16)$$

The mean flow is therefore given by $\bar{\mathbf{u}}(\mathbf{x}, t) = (\bar{u}(y, t), 0, 0)$ and $\bar{\phi}(\mathbf{x}, t) = \bar{\phi}(y, t)$.

Results and discussion

A snapshot of the simulation results is shown on Fig. 2. Noticeable is the multiscale nature of the liquid-gas interface which manifests in a variety of different liquid structures, e.g. three dimensional corrugations, detached ligaments and droplets. In this particular flow, droplets are known to be created from the rupture of ligaments which are ejected from the liquid bulk and stretched by the gas flow field [12]. Because stretch is responsible for the elongation of ligaments, one can therefore expect the transfer of $(\delta\phi')^2$ among the different scales to be a priori directed in the direction of large scales. Eq. (10) allows to provide greater details on this mechanism.

Here, given the symmetry of the flow, Eq. (10) 'reduces' to a problem in 5 dimensions with argument list (Y, r, t) . To reduce further the problem dimensionality, it is convenient to consider averaging the different terms of Eq. (10) over a sphere of radius $r = |\mathbf{r}|$ [6], viz.

$$\langle \beta \rangle_{\mathbb{S}}(\mathbf{X}, r, t) = \left(\frac{3}{4\pi r^3} \right) \iiint_{|\mathbf{r}'| \leq r} \beta(\mathbf{r}', \mathbf{X}, t) d\mathbf{r}' \quad (17)$$

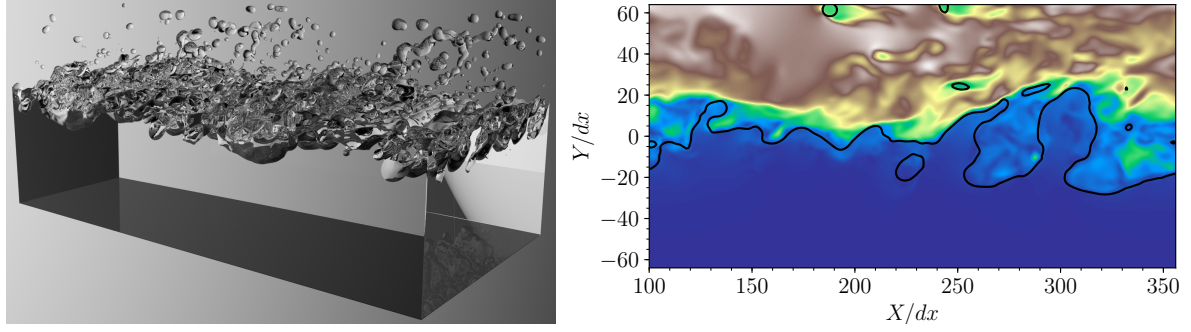


Figure 2. (left) Volume rendering of the liquid structures and (right) slice of the velocity magnitude and liquid-gas interface at a time $t = 1.76L_x/u_g$. The flow is directed from left to right.

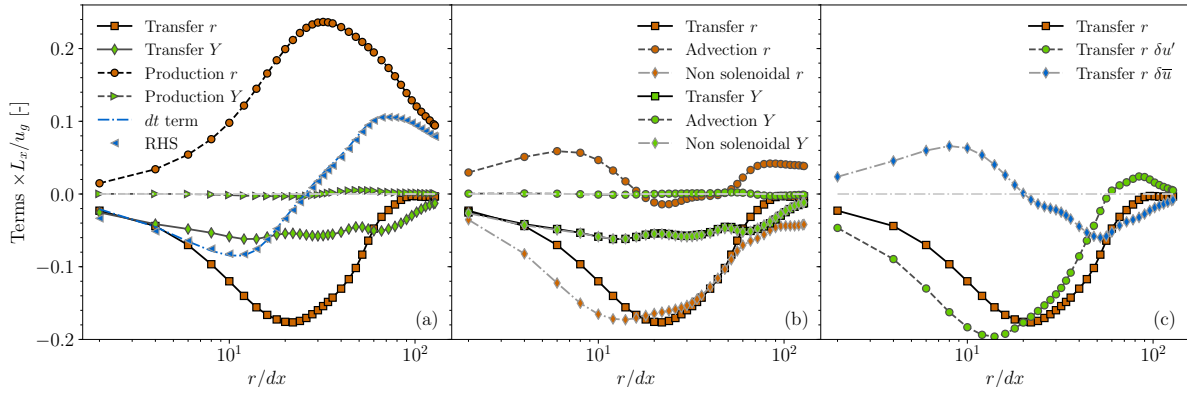


Figure 3. (a) Different terms of Eq. (18) normalized by u_g/L_x . (b) Decomposition of the r -transfer term into an advection and non-solenoidal term Eq. (13). (c) Decomposition of the r -transfer term into a mean and fluctuating component. Results are for $t = 1.76L_x/u_g$ and $Y = 0$

which, for the particular flow investigated here, leads to

$$\partial_t \left\langle \overline{(\delta\phi')^2} \right\rangle_{\mathcal{S}} = -\frac{3}{r} \left\langle \Phi_{\mathbf{r}} \cdot \frac{\mathbf{r}}{r} \right\rangle_{\partial\mathcal{S}} - \langle \nabla_Y \Phi_Y \rangle_{\mathcal{S}} - \langle \Pi_r \rangle_{\mathcal{S}} - \langle \Pi_Y \rangle_{\mathcal{S}} \quad (18)$$

where $\partial\mathcal{S}$ denotes the boundary of the averaging sphere and \mathbf{r}/r is the outwardly pointing normal to $\partial\mathcal{S}$. Therefore $\Phi_{\mathbf{r}} \cdot \mathbf{r}/r$ is the radial flux crossing $\partial\mathcal{S}$. By averaging over a sphere, the problem of VOF transport as given by Eq. (18) now depends on the vertical axis Y , the probed scale given by the sphere radius r and time. Note that the X -transfer and production term reduce to the ones in the vertical direction since, by homogeneity, $\nabla_X \bar{\beta} = \nabla_Z \bar{\beta} = 0$. In this form, one can now assess the direction and amplitude of the different mechanisms acting on the VOF field. For example, $\langle \Phi_{\mathbf{r}} \cdot \mathbf{r}/r \rangle_{\partial\mathcal{S}} > 0$ means that the flux is directed towards large scales. Similarly $\langle \nabla_Y \cdot \Phi_Y \rangle_{\mathcal{S}} > 0$ means that at a given plane perpendicular to Y , energy is transferred in the direction of increasing Y . Same reasoning applies to the productions terms.

The different terms of Eq. (18) at $Y = 0$ (i.e. on the center plane of the flow, $y = L_y/2$) and time $t = 1.76L_x/u_g$ are displayed on Fig. 3(a). One notes that the only positive term which thus acts as a gain in the budget is the r -production term. The latter peaks at a scale $r \approx 30 dx$ and tends to zero at either large and small scales. This indicates that mean quantities is feeding the fluctuating component of the liquid volume fraction field. The other significant term is the r -transfer which appears to be negative (a loss of energy) irrespectively of r . Therefore, on average, part of the energy available at a given scale is lost by being transferred towards large scales. This results confirms that at this position within the flow, liquid structures are positively stretched. The scale r at which the r -transfer term is maximum is about $20 dx$ which, interestingly, corresponds roughly to the size of ligaments observed in Fig. 2. Third, the transfer of energy in geometrical space ($-\langle \nabla_Y \Phi_Y \rangle_{\mathcal{S}}$) is also negative and represents about half the contribution of the r -transfer term. In other words, the energy transferred towards planes $> Y$ is larger than the one received from planes $< Y$, i.e. on average energy is transferred vertically. Finally, the Y -production term ($-\langle \Pi_Y \rangle_{\mathcal{S}}$) is negligible. The sum of all aforementioned contributions should equate the time derivative term for Eq. (18) to be verified. Here, comparing the dt -term to the RHS Eq. (18) on Fig. 3(a) reveals that the budget is very closely satisfied. This is a very nice test to assess the appropriateness of a DNS. Any departure from this budget indicates that either the resolution or the numerical method is inaccurate. To summarize, the dt -term in Fig. 3(a) reveals two distinct behaviour. At large scales (i.e. $r > r^* \approx 15 dx$), the dt -term is positive and the energy is increasing due to the prominent role of the production mechanism. At small scales (i.e. $r < r^* \approx 15 dx$), the dt -term is negative and energy is lost through a transfer process towards larger scales (positive stretch) and towards planes of greater altitude.

On Fig. 3(b) is displayed the r - and Y -transfer terms once decomposed into a pure advection and a sink/source

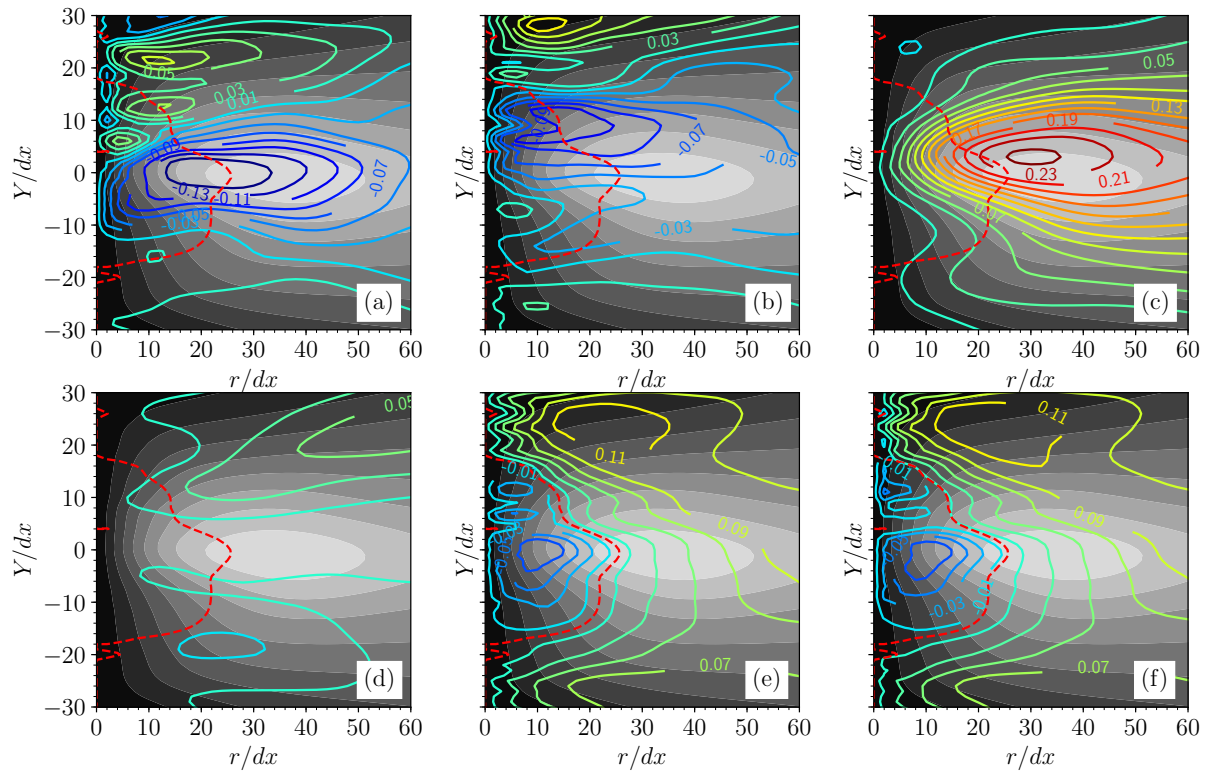


Figure 4. Different terms of the budget of $\langle (\delta\phi')^2 \rangle_s$ (black filled contours) in the (Y, r) plane at a time $t = 1.76L_x/u_g$. Are displayed as contours (a) the r -Transfer term, (b) the Y -Transfer term, (c) the r -Production term, (d) the Y -Production term, (e) the dt term and (f) the RHS. The dashed red contour corresponds to r, Y at which the dt -term is zero. Terms are normalized by u_g/L_x

term as given by Eq. (13). In scale space, one notes on Fig. 3(b) that the advection mechanism is positive at small scales meaning that energy is advected in the direction of smaller scales. On the contrary, the sink/source term is positive with a much higher contribution. As far as the Y -transfer term is concerned, it appears that only the sink/source term contribute, the advection term w_Y being negligible. One immediate conclusion is that non-local interactions predominates in this flow.

Finally, one should further consider the decomposition of the r -transfer term into a contribution due to the mean and fluctuating flow field, respectively (see Eq. (11)). Note that such a decomposition is irrelevant for the Y -transfer since $\sigma\bar{v} = 0$ and thus $\overline{\sigma v (\delta\phi')^2} = \overline{\sigma v' (\delta\phi')^2}$. Results are presented on Fig. 3(c). In this flow field, inhomogeneity of the mean flow field is stronger than that of the fluctuating counterpart. As a consequence, it is not surprising to observe that the transfer term is dominated by the contribution of the mean flow field. Another interesting observation can be drawn by comparing Fig. 3(b) and Fig. 3(c). Indeed, it appears that at small scales ($r \lesssim 20dx$), the r -advection term in Fig. 3(b) closely matches the fluctuating contribution to the transfer in Fig. 3(c), while the source term in Fig. 3(b) is similar to the mean velocity transfer term in Fig. 3(c). This means that on average, the mean flow field is responsible for the elongation of liquid structures while turbulent fluctuations are more prone to accentuate a cascade of energy towards smaller scales. Second, this observations indicates that non-local interactions are carried by the mean field while turbulent fluctuations are responsible for local transfers of energy.

Eq. (18) is now analysed at different planes Y and as a function of the sphere radius r . In Fig. 4(a-f) are portrayed the scale 'energy' $\langle (\delta\phi')^2 \rangle_s$ and the different terms which constitute Eq. (18). Also represented as the red dashed line is the scale $r^*(Y)$ for which the time derivative term is zero. The dt -term is negative (positive) for $r < r^*$ ($r > r^*$). As it was noticed earlier for $Y = 0$, the range of scales over which energy decays ($r < r^*$) is dominated by the r - and Y -transfer term. This region ($-20 dx \lesssim Y \lesssim 20 dx, r < r^*$) is therefore characterized by a strong positive stretch (Fig. 4(a)) and strong vertical flux (Fig. 4(b)). It is further worth noting that for $Y > 20 dx$, the r -transfer process is positive, revealing that energy cascades towards smaller scales. The r -production term (Fig. 4(c)) is positive throughout the domain, with a peak value located around the center plane of flow and a scale $r \approx 30 dx$. For scales $r > r^*$, this term represents the prominent contribution. Here again, comparing Figs. 4(e) and (f) shows that Eq. (18) is very nicely satisfied.

The application of the spherical average has virtually hidden the processes (transfer, production) that may have occurred between different orientations of the vector r . This point is thus further addressed now. For this purpose we plot in Fig. 5 the energy content of the fluctuating field $\overline{(\delta\phi')^2}$ and the direction and amplitude of the convection velocity $w_{r,x}$ in some different sub-manifolds. These figures reveal the very complex nature of energy transfer in this particular flow field. The strong inhomogeneity of the flow in Y -direction induces a strong anisotropy of energy transfer, i.e. statistics depends on the orientation of the separation vector r . In Fig. 5(a-c), we observe that a

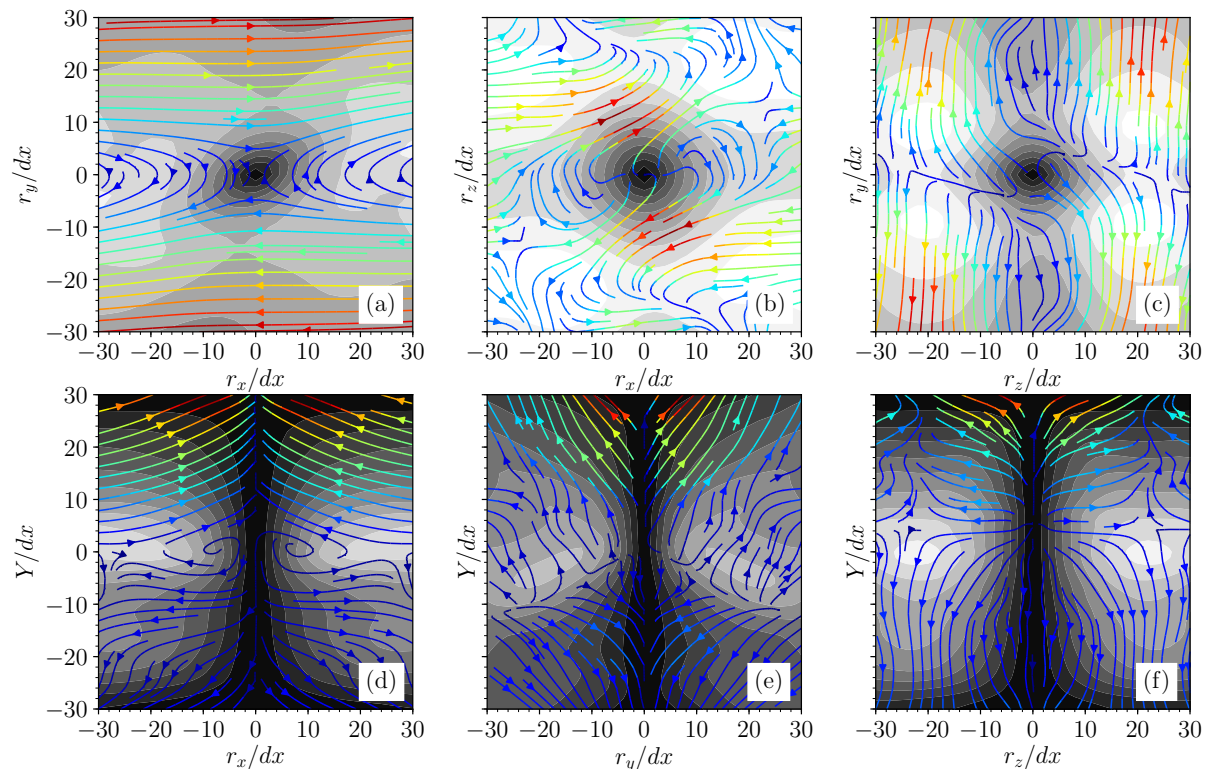


Figure 5. Slices of $\overline{(\delta\phi)^2}$ (black filled contours) and $w_{r,x}$ (streamlines) in (a) the $(r_x, r_y, 0, 0)$ plane, (b) the $(r_x, 0, r_z, 0)$ plane, (c) the $(0, r_y, r_z, 0)$ plane, (d) the $(r_x, 0, 0, Y)$ plane, (e) the $(0, r_y, 0, Y)$ plane and (f) the $(0, 0, r_z, Y)$ plane. Streamlines are coloured by the magnitude of $w_{r,x}$.

large amount of energy is transferred towards large scales, especially in the r_x and r_y directions. As stated earlier, this is representative of the elongation of liquid structures in these particular directions. The streamlines plotted in Fig. 5(a) also show that a significant part of the energy transfer is associated with a tilting of liquid structures in the clockwise direction, i.e. structures being stretched vertically rotate and tend to align with the r_x axis. Finally, Figs. 5(d-f) indicates the fluxes passing through different vertical planes for different orientations of the vector r . It is observed that the vertical flux is significant in regions corresponding to $Y > 10 - 30 dx$, i.e. the region where the Y - and r -transfer terms contribute positively. In the (Y, r_x) plane (Fig. 5(a)) streamlines are directed towards smaller scales. This is interpreted as being representative of the contraction of ligaments and/or the break-up of such ligaments into droplets.

Conclusions

With the aim of exploring the multiscale nature of turbulent two-phase flows, a new theoretical framework inherited from the single-phase turbulence community [1, 2, 6, 8, 15] is proposed. It relies on the liquid volume fraction transport equation which is written at two-points arbitrary separated by a distance r . By doing so, the transport of liquid is shown to depend on a transfer and a production process which act together and concomitantly in physical space (i.e. from one position in the flow to the other) and in scale space (e.g. from large to small or vice-versa). We have also pointed out the co-existence of local and non-local interactions between different scales and positions. This new framework is exact as long as the flow remains incompressible with no-phase change. It is therefore a nicely tailored tool to appraise the appropriateness of a given numerical simulation method and resolution. The notion of scale is explicit and unambiguously defined. It applies to the entire flow field, from the injection to the spray dispersion zone and irrespectively of the flow configuration or regime. It allows exploring notably the direction and amplitude of the transfer among the different scales and the effect of different physical parameters (surface tension, viscosity and density, inflow velocity conditions), and the range of scales over which these parameters have an influence. Consequently, transposing the two-point statistical analysis to ϕ appears particularly promising for providing insights into the complex physics of liquid atomization. Note however that this framework is only an exploratory tool, but is incapable of predictions as the sequential cascade [4, 11], the aggregation [23, 12] or the maximum entropy [18, 3] phenomenologies can provide. The reason is that Eq. (10) is not closed, i.e. the transport of second-order statistics depends on higher order terms.

Here, a DNS dataset of a planar liquid layer being sheared by a gas stream is used to quantify the different terms of the new two-point equation. It is archetypal of a type of atomization configuration generally referred to as the air-assisted atomization process. This particular flow is statistically symmetric (homogeneous) in the spanwise and streamwise direction so that the full set of equations relies on a 5 dimensional manifold.

The most important conclusion to be drawn is that the transfer of liquid between different scales can be either positive

(towards small scales) or negative (large scales) depending on the probed scale and vertical plane. Negative transfer is here attributed to a positive stretch of liquid structures (elongation), positive transfer corresponding to their contraction or break up. Therefore, there exist some region in the flow and some scales complying predominantly either with the cascade scenario [4, 11], or with the aggregation scenario [23, 12]. It is also worth pointing out the role of production of liquid volume fraction fluctuations associated with the correlation between the vertical component of the velocity field and the ϕ field. This term dominates over a wide region of the flow. Finally, exploring the nature of energy fluxes within different sub-planes of the full manifold have allowed us emphasizing the tilting process within different orientation of the separation vector r . This process is interpreted as being representative of the rotation of liquid structures.

Acknowledgements

We are thankful to A. Poux, research engineer at CORIA laboratory for having optimized the calculation of the increments. Computations have been carried out in CRIANN (Centre Régional Informatique et d'Applications Numériques de Normandie) under the project 2018002. FT also benefited from the financial support from the INSIS institute of the CNRS which is gratefully acknowledged.

References

- [1] L Danaila, F Anselmet, T Zhou, and RA Antonia. A generalization of Yaglom's equation which accounts for the large-scale forcing in heated decaying turbulence. *J. Fluid Mech.*, 391:359–372, 1999.
- [2] L Danaila, RA Antonia, and P Burattini. Progress in studying small-scale turbulence using 'exact' two-point equations. *New Journal of Physics*, 6(1):128, 2004.
- [3] C Dumouchel. The maximum entropy formalism and the prediction of liquid spray drop-size distribution. *Entropy*, 11(4):713–747, 2009.
- [4] MA Gorokhovski and VL Saveliev. Analyses of Kolmogorov's model of breakup and its application into Lagrangian computation of liquid sprays under air-blast atomization. *Phys. Fluids*, 15(1):184–192, 2003.
- [5] M Herrmann and M Gorokhovski. An outline of a LES subgrid model for liquid/gas phase interface dynamics. *Proceedings of the 2008 CTR Summer Program*, pages 171–181, 2008.
- [6] RJ Hill. Exact second-order structure-function relationships. *J. Fluid Mech.*, 468:317–326, 2002.
- [7] CW Hirt and BD Nichols. Volume of fluid (VOF) method for the dynamics of free boundaries. *J Comput Phys*, 39(1):201–225, 1981.
- [8] T Kármán and L Howarth. On the statistical theory of isotropic turbulence. *Proc. Roy. Soc. Lond. A*, 164(917):192–215, 1938.
- [9] A N Kolmogorov. Dissipation of energy in locally isotropic turbulence. *Dokl. Akad. Nauk SSSR*, 32(1):16–18, 1941.
- [10] AN Kolmogorov. The local structure of turbulence in incompressible viscous fluid for very large Reynolds numbers. *Dokl. Akad. Nauk SSSR*, 30(4):299–303, 1941.
- [11] AN Kolmogorov. On the log-normal law of distribution of particles during fragmentation. *Dokl. Akad. Nauk SSSR*, pages 99–101, 1941.
- [12] Ph Marmottant and E Villermaux. On spray formation. *J Fluid Mech*, 498:73–111, 2004.
- [13] JO McCaslin and O Desjardins. Theoretical and computational modeling of turbulence/interface interactions. In *Proceedings of the Summer Program*, page 79, 2014.
- [14] T. Ménard, S. Tanguy, and A. Berlemont. Coupling level set/VOF/ghost fluid methods: Validation and application to 3D simulation of the primary break-up of a liquid jet. *Int. J. Multiphase Flow*, 33(5):510–524, may 2007.
- [15] J-P Mollicone, F Battista, P Gualtieri, and CM Casciola. Turbulence dynamics in separated flows: the generalised Kolmogorov equation for inhomogeneous anisotropic conditions. *J. Fluid Mech.*, 841:1012–1039, 2018.
- [16] LF Richardson. The supply of energy from and to atmospheric eddies. *Proc. R. Soc. Lond. A*, 97(686):354–373, 1920.
- [17] R Scardovelli and S Zaleski. Direct numerical simulation of free-surface and interfacial flow. *Annu Rev Fluid Mech*, 31(1):567–603, 1999.
- [18] RW Sellens and TA Brzustowski. A simplified prediction of droplet velocity distributions in a spray. *Combust Flame*, 65(3):273–279, 1986.
- [19] R Togni, A Cimarelli, and E De Angelis. Physical and scale-by-scale analysis of Rayleigh–Bénard convection. *J. Fluid Mech.*, 782:380–404, 2015.
- [20] A. Tsinober. *An informal conceptual introduction to turbulence (Second Edition of An Informal Introduction to Turbulence)*. Springer Science & Business Media, 2009.
- [21] G Vaudor, T Ménard, W Aniszewski, M Doring, and A Berlemont. A consistent mass and momentum flux computation method for two phase flows. application to atomization process. *Computers & Fluids*, 152:204–216, 2017.
- [22] E Villermaux. Fragmentation. *Annu. Rev. Fluid Mech.*, 39:419–446, 2007.
- [23] E Villermaux, Ph Marmottant, and J Duplat. Ligament-mediated spray formation. *Phys Rev Lett*, 92(7):074501, 2004.
- [24] AM Yaglom. On the local structure of a temperature field in a turbulent flow. *Dokl. Akad. Nauk SSSR*, 69(6):743–746, 1949.